

<https://doi.org/10.1038/s42003-024-06897-w>

Blockade of Crk eliminates Yki/YAP-activated tumors via JNK-mediated apoptosis in *Drosophila*

Check for updates

Bungo Kakemura & Tatsushi Igaki

Selective elimination of cancer cells without causing deleterious effects on normal cells is an ideal anti-cancer strategy. Here, using *Drosophila* cancer model, we performed an in vivo RNAi screen for anti-cancer targets that selectively eliminate tumors without affecting normal tissue growth. In *Drosophila* imaginal epithelium, clones of cells expressing oncogenic Ras with simultaneous mutations in the cell polarity gene *scribble* (*Ras*^{V12}/*scrib*^{-/-}) develop into malignant tumors. We found that knockdown of *Crk*, the *Drosophila* ortholog of human CRK (CT10 regulatory kinase) and CRKL (Crk-like) adapter proteins, significantly suppresses growth of *Ras*^{V12}/*scrib*^{-/-} tumors by inducing c-Jun N-terminal kinase (JNK)-mediated apoptosis, while it does not affect growth of normal epithelium.

Mechanistically, Crk inhibition blocks Yorkie (Yki)/YAP activity by impairing F-actin accumulation, an upstream event of Yki/YAP activation in tumors. Inhibition of Yki/YAP in tumors causes intracellular JNK signaling to be used for apoptosis induction. Given that molecules and signaling pathways identified in *Drosophila* are highly conserved and activated in human cancers, our findings would provide a novel, to the best of our knowledge, anti-cancer strategy against YAP-activated cancers.

An ideal strategy against cancer is selective elimination of cancer cells without causing deleterious effects on normal cells. One such approach is the inhibition of signaling molecule that is specifically contributing to cancer cell proliferation or survival. It is therefore crucial to identify such specific target molecules in cancer cells. However, the complexity of using in vivo models of mammalian cancers has hampered the systematic identification of target molecules that can manipulate cancer cells.

Drosophila serves as an ideal in vivo platform for identifying molecules that are specifically required for cancer cell proliferation or survival¹⁻³. The genetic mosaic technique available in *Drosophila*⁴ allows us to dissect the signaling network within tumors and identify tumor-specific proliferation or survival signaling by tumor-specific genetic manipulations or gene silencing. In *Drosophila* imaginal epithelia, genetic mosaic clones of cells expressing oncogenic Ras (*Ras*^{V12}) with simultaneous mutations in apico-basal cell polarity gene *scribble* (*scrib*) develop into malignant tumors⁵. The *Ras*^{V12}/*scrib*^{-/-} tumors exhibit human cancer-like phenotypes such as tumor overgrowth, invasion, metastasis, and ultimately animal death⁵⁻⁷, providing an ideal genetic model to study tumor growth and progression.

YAP (YES-associated protein 1) is a transcriptional co-activator implicated in cancer initiation, progression, and invasion⁸. YAP activity is frequently elevated in various types of cancer⁹ and thus YAP and its

upstream regulatory molecules can be therapeutic targets against cancer¹⁰⁻¹². *Drosophila* possesses the YAP homolog Yorkie (Yki), which functions as an oncogene that enhances cell proliferation and promotes cell survival¹³. Since the function of YAP and its upstream regulatory molecules are well conserved in *Drosophila*¹⁴, identification of molecules that effectively manipulate Yki-activated tumors in *Drosophila* would provide new strategies against YAP-activated cancers in humans.

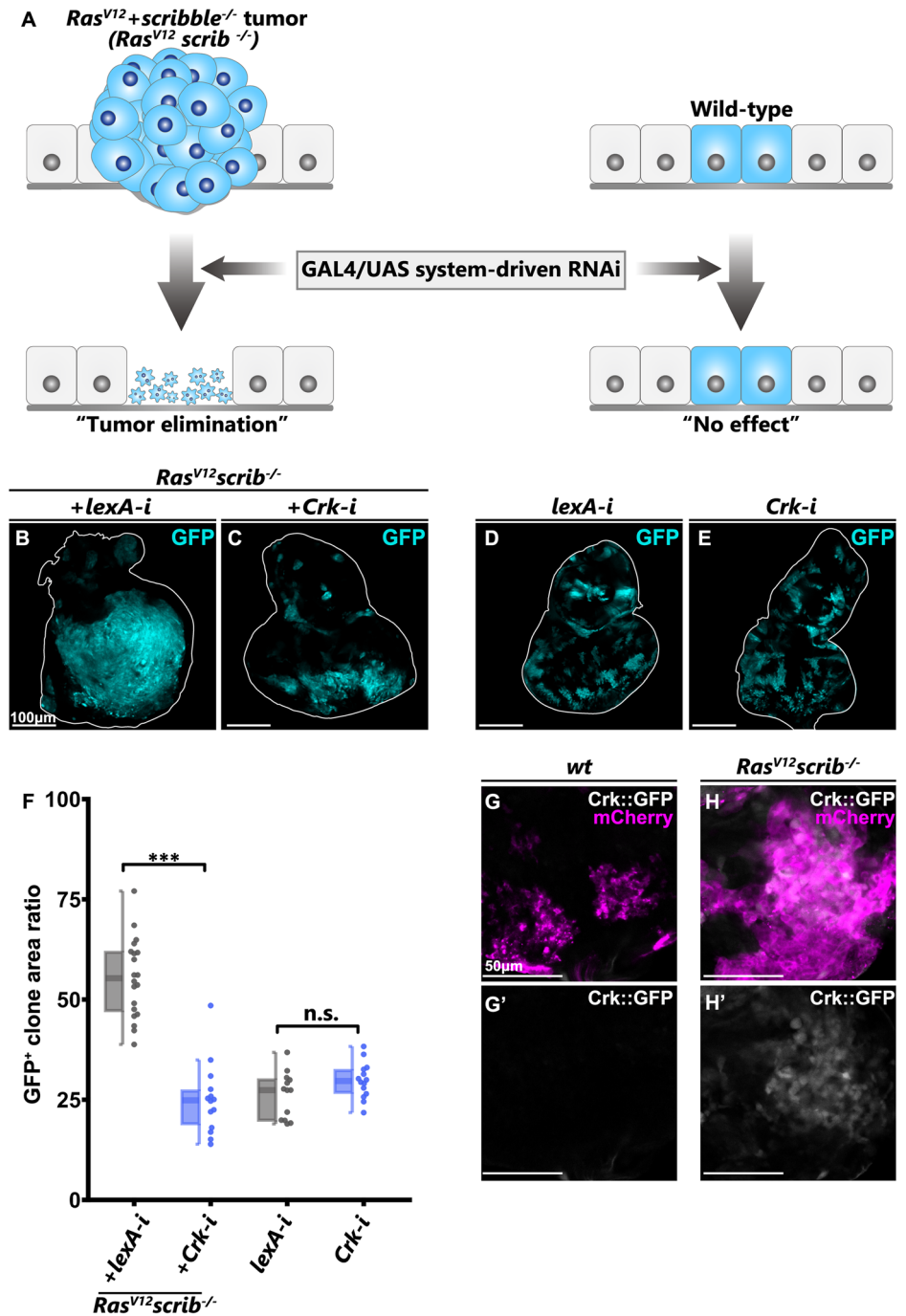
Human CRK (CT10 regulatory kinase) and CRKL (CRK-like) are adaptor proteins composed of SH2 and SH3 domains, which regulate various cellular processes such as cell motility, adhesion, and proliferation^{15,16}. Expression of CRK or CRKL is elevated in various types of cancers and contributes to tumor growth^{17,18}. Hence CRK and CRKL have gained attention for their potential as targets for cancer therapy¹⁷. However, the presence of two CRK isoforms (CRK-I, CRK-II) and functional redundancy between CRK and CRKL have hampered the in vivo analysis of these proteins in cancer. *Drosophila* has a single orthologue of the CRK family of proteins¹⁹. Therefore, the use of *Drosophila* would provide a great advantage in understanding the in vivo role of CRK family proteins in cancer.

Here, by conducting an in vivo RNAi screen using the *Drosophila* *Ras*^{V12}/*scrib*^{-/-} malignant tumor model, we identified Crk as a potent anti-cancer target with a negligible effect on normal cells. Loss of Crk had little

Laboratory of Genetics, Graduate School of Biostudies, Kyoto University, 46-29, Yoshida-shimoadachi-cho, Sakyo-ku, Kyoto, 606-8501, Japan.

 e-mail: igaki.tatsushi.4s@kyoto-u.ac.jp

Fig. 1 | A genetic screen identifies Crk as a selective tumor suppressor. **A** Genetic screen with a series of RNAi strains to identify tumor-suppressor strains. Using the mosaic analysis system (MARCM), Ras-activated cell clones bearing *scribble* mutation ($Ras^{V12}/scrib^{-/-}$ tumor) were generated in larval eye-antennal discs. RNAi strains that suppressed tumorigenesis when induced into those tumors were isolated as tumor-suppressor strains. **B–E** The eye-antennal discs bearing eyFLP-induced MARCM clones. The upper direction of each image is the antenna side. Transgene expression or knocking down is induced inside GFP-positive clones under Gal4-UAS system, and each clone genotype is described upper each image. Eye disc bearing eyFLP-induced MARCM clones of $Ras^{V12} + scrib^{-/-} + lexA-i$ (**B**), $Ras^{V12} + scrib^{-/-} + Crk-i$ (**C**), $lexA-i$ (**D**), $Crk-i$ (**E**), cells. Dissections of tumor-bearing larvae were performed at day 7 after egg laying. Scale bars, 100 μ m. **F** Box plot overlaid with dot plot represents the total GFP-positive clone area per total disc area (the proportion of total clone area/ disc area) for $Ras^{V12} + scrib^{-/-} + lexA-i$ ($n = 20$), $Ras^{V12} + scrib^{-/-} + Crk-i$ ($n = 14$), $lexA-i$ ($n = 13$), $Crk-i$ ($n = 14$) clones. Each plot corresponds to the raw data. Statistical significance is shown as follows: *** $p < 0.001$; n.s. (not significant) $p > 0.05$; Wilcoxon rank sum test. **G, H** Eye disc bearing eyFLP-induced MARCM clones and Crk::GFP heterozygously of wild-type (**G**), $Ras^{V12} + scrib^{-/-}$ (**H**) cells stained with anti-GFP. Scale bars, 50 μ m.



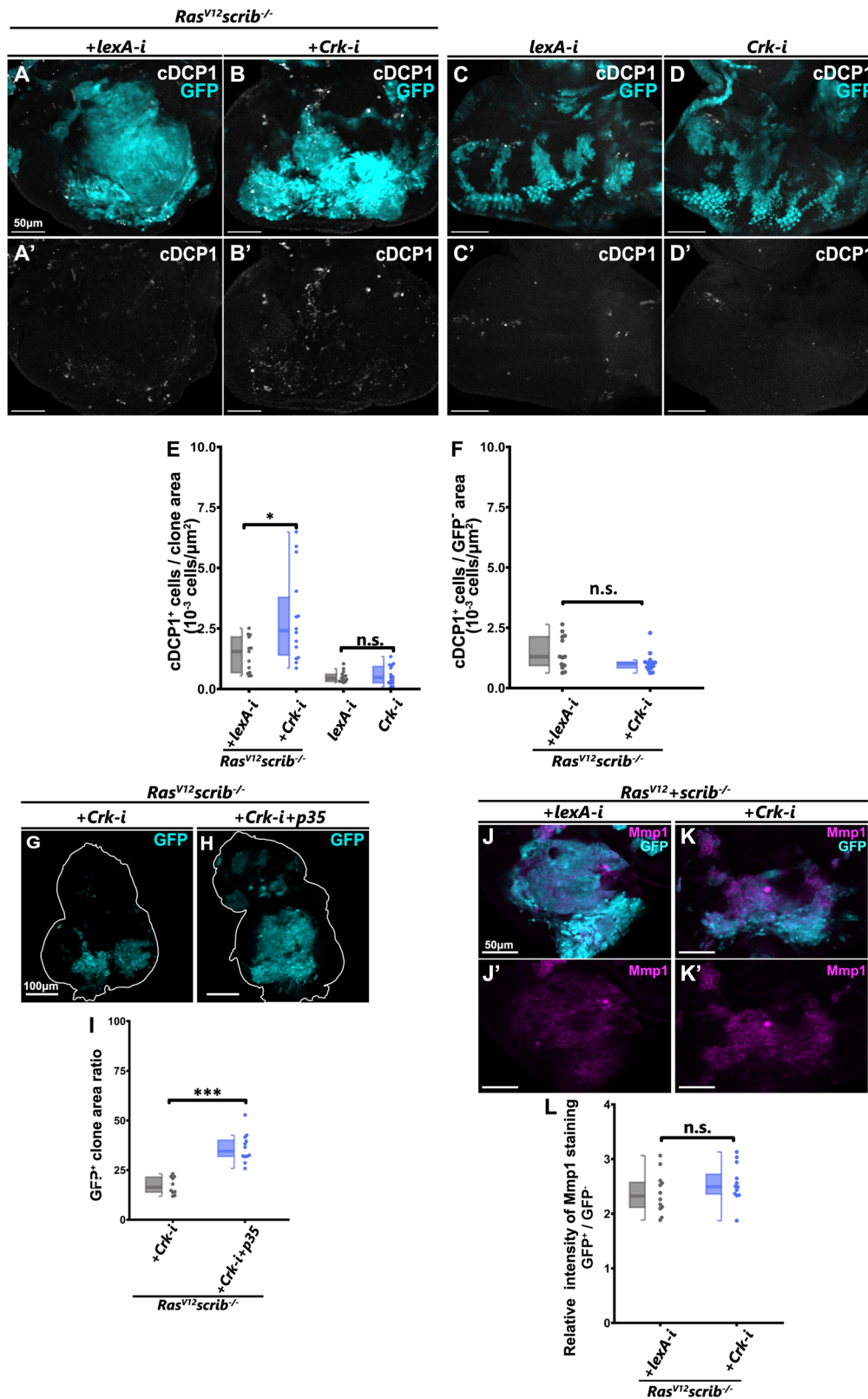
effect on normal tissue growth but eradicated $Ras^{V12}/scrib^{-/-}$ tumors by increasing apoptosis. Subsequent genetic analyses revealed that Crk inhibition impairs F-actin accumulation in $Ras^{V12}/scrib^{-/-}$ tumors, which leads to suppression of Yki/YAP activation. Analysis of the human cancer database revealed that YAP-activated cancers are sensitive to loss of CRK family proteins. Our genetic data in *Drosophila*, in conjunction with the database analysis in human cancers, could provide an effective therapeutic strategy against YAP-activated human cancers.

Results

Identification of Crk as a potential target for selective tumor elimination

To identify potential target molecules for selective tumor elimination, we conducted an in vivo RNAi screen using a well established *Drosophila* $Ras^{V12}/scrib^{-/-}$ malignant tumor model. Using the Flippase (FLP)-FLP

recognition target (FRT)-mediated genetic mosaic technique^{4,20}, GFP-labeled $Ras^{V12}/scrib^{-/-}$ tumors were generated in the larval eye-antennal discs and a series of RNAis against the genes on the chromosome 4, which have not been systematically investigated by genetic screens, was simultaneously introduced in the tumors (Fig. 1A, see Supplementary Table 1). Among 57 genes screened, we found that knockdown of *Crk* in $Ras^{V12}/scrib^{-/-}$ tumor clones strongly suppressed tumor growth (Fig. 1C, compare to B, quantified in F). Similarly, *Crk* knockdown strongly suppressed growth of $Ras^{V12}/dlg^{-/-}$ tumors, another well-established malignant tumor model in *Drosophila*^{5,21} (Supplementary Fig. 1B, compare to A, quantified in C). Notably, *Crk* knockdown did not affect growth of wild-type clones (Fig. 1E, compare to D, quantified in F). We further found that the Crk protein level was elevated in $Ras^{V12}/scrib^{-/-}$ tumors compared to wild-type tissue (Fig. 1H, compare to G). Notably, neither Ras^{V12} -expressing cells



nor *scrib*^{-/-} cells elevated the Crk protein level (Supplementary Fig. 2A, B). In addition, overexpression of Crk or simultaneous overexpression of Crk and Ras^{V12} did not cause overgrowth (Supplementary Fig. 3A–D, quantified in E). These data suggest that Ras^{V12}/*scrib*^{-/-} tumors overgrow by elevating Crk, which is a potential target for selective elimination of tumors.

Loss of Crk reduces Ras^{V12}/*scrib*^{-/-} tumor size by increased apoptosis

We next investigated the mechanism by which *Crk* knockdown reduces Ras^{V12}/*scrib*^{-/-} tumor size. We found that *Crk* knockdown increased cell death in Ras^{V12}/*scrib*^{-/-} tumors (Fig. 2B, compare to A, quantified in E), while it did not increase cell death in wild-type tissue (Fig. 2D, compare to C,

Fig. 2 | Loss of Crk increases apoptosis in a JNK-dependent manner in $Ras^{V12}/scrib^{-/-}$ tumors. **A–D** Eye disc bearing eyFLP-induced MARCM clones of $Ras^{V12} + scrib^{-/-} + lexA-i$ (A), $Ras^{V12} + scrib^{-/-} + Crk-i$ (B), $lexA-i$ (C), $Crk-i$ (D) cells stained with anti-cleaved Dcp-1. Scale bars, 50 μ m. **E** Box plot overlaid with dot plot represents the number of c-Dcp1 positive cells in $Ras^{V12} + scrib^{-/-} + lexA-i$ (n = 13), $Ras^{V12} + scrib^{-/-} + Crk-i$ (n = 14), $lexA-i$ (n = 13), $Crk-i$ (n = 15) cells. Each plot corresponds to the raw data. Statistical significance is shown as follows: * $p < 0.05$; n.s. (not significant) $p > 0.05$; Wilcoxon rank sum test. **F** Box plot overlaid with dot plot represents the number of c-Dcp1 positive cells in GFP negative area of the tissue bearing $Ras^{V12} + scrib^{-/-} + lexA-i$ (n = 13), $Ras^{V12} + scrib^{-/-} + Crk-i$ (n = 14) cells. Each plot corresponds to the raw data. Statistical significance is shown as follows: n.s. (not significant) $p > 0.05$; Wilcoxon rank sum test. **G, H** Eye disc bearing eyFLP-

induced MARCM clones of $Ras^{V12} + scrib^{-/-} + Crk-i$ (G), $Ras^{V12} + scrib^{-/-} + Crk-i + p35$ (H) cells. Scale bars, 100 μ m. **I** Box plot overlaid with dot plot represents the total GFP-positive clone area per total disc area (the proportion of total clone area/disc area of the eye-antennal disc) for $Ras^{V12} + scrib^{-/-} + Crk-i$ (n = 10), $Ras^{V12} + scrib^{-/-} + Crk-i + p35$ (n = 12) cells. Each plot corresponds to the raw data. Statistical significance is shown as follows: *** $p < 0.001$; Wilcoxon rank sum test. **J, K** Eye disc bearing eyFLP-induced MARCM clones of $Ras^{V12} + scrib^{-/-} + lexA-i$ (J), $Ras^{V12} + scrib^{-/-} + Crk-i$ (K), cells stained with anti-Mmp1. Scale bars, 50 μ m. **L** Box plot overlaid with dot plot represents the relative Mmp1 intensity in clone for $Ras^{V12} + scrib^{-/-} + lexA-i$ (n = 12), $Ras^{V12} + scrib^{-/-} + Crk-i$ (n = 12) clones. Each plot corresponds to the raw data. Statistical significance is shown as follows: n.s. (not significant) $p > 0.05$; Wilcoxon rank sum test.

quantified in E). *Crk* knockdown did not affect cell death in GFP-negative area (Fig. 2B, compare to A, quantified in F). Consistent with these observations, the reduction in $Ras^{V12}/scrib^{-/-}$ tumor size by *Crk* knockdown was cancelled by co-expression of the caspase inhibitor p35 (Fig. 2H, compare to G, quantified in I). Given that JNK signaling is a major signaling that regulates both tumor growth and apoptosis depending on the cellular context and that JNK is activated in $Ras^{V12}/scrib^{-/-}$ tumors²², we hypothesized that tumor reduction by *Crk* knockdown is mediated by JNK signaling. Indeed, inhibition of JNK signaling by overexpression of a dominant-negative form of *Drosophila* JNK Basket (*Bsk*^{DN}) decreased cell death in $Ras^{V12}/scrib^{-/-}$ tumors with *Crk* knockdown (Supplementary Fig. 4B, compare to A, quantified in C). Intriguingly, cell death in GFP-negative area was also slightly suppressed when JNK was blocked in $Ras^{V12}/scrib^{-/-}$ tumors by *Crk* knockdown (Supplementary Fig. 4B, compare to A, quantified in D), which could possibly be due to the induction of apoptosis-induced apoptosis caused by *Drosophila* TNF ligand Eiger (*Egr*)^{23,24}-JNK signaling, which is known to be activated in $Ras^{V12}/scrib^{-/-}$ tumors²⁵. We found that JNK signaling activity in $Ras^{V12}/scrib^{-/-}$ tumors was not increased by *Crk* knockdown, as visualized by the JNK-target anti-Mmp1 staining²² or anti-phospho-JNK (pJNK) staining (Fig. 2K, compare to J, quantified in L, Supplementary Fig. 5B, compare to A, quantified in C), suggesting that JNK promotes apoptosis when *Crk* is blocked in $Ras^{V12}/scrib^{-/-}$ tumors. These data indicate that *Crk* knockdown reduces $Ras^{V12}/scrib^{-/-}$ tumor size by increased apoptosis in a JNK-dependent manner.

Loss of Crk downregulates Yki activity in $Ras^{V12}/scrib^{-/-}$ tumors

A possible mechanism by which *Crk* knockdown increases JNK-dependent cell death in $Ras^{V12}/scrib^{-/-}$ tumors is an inhibition of a tumor-specific survival factor. One such candidate is Yki, a downstream effector of Hippo signaling that promotes tissue growth by enhancing cell proliferation and blocking apoptosis. Indeed, it has been shown that Yki contributes to $Ras^{V12}/scrib^{-/-}$ tumor growth^{21,26,27}. Notably, *Crk* knockdown in $Ras^{V12}/scrib^{-/-}$ tumors significantly suppressed Yki activity, as visualized by the Yki activity reporter *diap1-lacZ* (a transcriptional target of Yki-Sd)¹³ (Fig. 3B, compare to A, quantified in E), while it did not affect the endogenous Yki activity in wild-type cells (Fig. 3D, compare to C, quantified in E). This was further confirmed using the *ex-lacZ* reporter, another target of Yki²⁸, which was suppressed by *Crk* knockdown in $Ras^{V12}/scrib^{-/-}$ tumors (Supplementary Fig. 6B, compare to A, quantified in C). We found that cell proliferation in $Ras^{V12}/scrib^{-/-}$ tumors was also slightly suppressed by *Crk* knockdown (Supplementary Fig. 7B, compare to A, quantified in C), which is consistent with the observation that *Crk* knockdown suppresses Yki activity. Consistent with these data, knockdown of *yki* in $Ras^{V12}/scrib^{-/-}$ tumors significantly increased apoptosis (Fig. 3G, compare to F, quantified in H). These lines of evidence suggest that *Crk* knockdown downregulates Yki activity specifically in $Ras^{V12}/scrib^{-/-}$ tumors, thereby eliminates tumors by inducing JNK-dependent apoptosis.

Loss of Crk suppresses Yki activity by blocking F-actin accumulation

We next sought to clarify the mechanism by which *Crk* knockdown downregulates Yki activity in $Ras^{V12}/scrib^{-/-}$ tumors. It has been reported that *Drosophila* Crk regulates actin dynamics during normal

development¹⁹. In addition, intracellular F-actin accumulation causes Yki activation via inactivation of the Hippo pathway²⁹. Particularly, elevated Ras signaling in conjunction with JNK activation leads to accumulation of F-actin, thereby causing Yki activation²⁹. Significantly, we found that *Crk* knockdown diminished the accumulation of intracellular F-actin in $Ras^{V12}/scrib^{-/-}$ tumors (Fig. 4B, compare to A, quantified in E, also see Supplementary Fig. 8). Furthermore, *Crk* knockdown also abolished F-actin accumulation in tumor clones bearing elevated Ras and JNK activity, which was induced by co-expression of Ras^{V12} and *Egr* (Fig. 4D, compare to C quantified in F). Consistently, *Crk* knockdown significantly suppressed growth of Ras^{V12}/Egr tumors (Fig. 4H, compare to G, quantified in M). Notably, *Crk* knockdown suppressed neither growth (Fig. 4J, compare to I, quantified in M) nor F-actin accumulation (Supplementary Fig. 9D, compare to C, quantified in F) of Yki-activated tumors induced by overexpression of a constitutively activated form Yki (*Yki*^{S168A})^{30,31}. These results are consistent with the notion that *Crk* knockdown blocks F-actin accumulation, which is the upstream event of Yki activation. Similarly, *Crk* knockdown affected neither growth (Fig. 4L, compare to K, quantified in M) nor F-actin accumulation (Supplementary Fig. 9B, compare to A, quantified in E) of Ras^{V12} -expressing tumors. Collectively, these data suggest that *Crk* knockdown in $Ras^{V12}/scrib^{-/-}$ tumors blocks Yki activity by downregulating the Ras/JNK-mediated accumulation of intracellular F-actin, thereby increasing JNK-dependent apoptosis and thus eliminating tumors.

YAP-activated human cancers are sensitive to loss of CRK family proteins

Finally, we investigated whether the mechanism identified in the *Drosophila* model can be applicable to human cancer suppression. We exploited the database of the Cancer Dependency Map project (DepMap portal: <https://depmap.org/portal>), an ongoing project that assesses the gene essentiality for cancer cells by genome-wide RNAi and CRISPR screens^{32,33}. The gene essentiality score is shown as a dependency score, the negative value of which reflects decreased proliferation of cancer cells by the CRISPR-Cas9-mediated gene knockout or RNAi-mediated gene silencing. We first assessed the co-dependency (i.e., the positive correlation of dependency scores) of CRK family proteins and YAP. Remarkably, CRK and CRKL are co-dependent with YAP in both CRISPR screen (DepMap Public 22Q4+Score, Chronos) and RNAi screen (Achilles+DRIVE+Marcotte, DEMETER2) projects (Fig. 5A, see 'Pearson correlation'), suggesting that YAP-activated cancer cells are also sensitive to loss of CRK or CRKL. Moreover, we found that the expression levels of YAP mRNA (Fig. 5B–E) or YAP protein (Fig. 5F–I) show significant negative correlation with CRK or CRKL gene effect, indicating that cells highly expressing YAP are sensitive to gene knockout or gene silencing of CRK or CRKL. These data suggest that the critical role of CRK family proteins in Yki/YAP activation in tumor cells, which was uncovered by our genetic study in *Drosophila*, could be conserved in human cancers.

Discussion

In this study, we identified *Drosophila* Crk as a potential therapeutic target for Yki/YAP-activated tumors. Our genetic data revealed that Crk inhibition

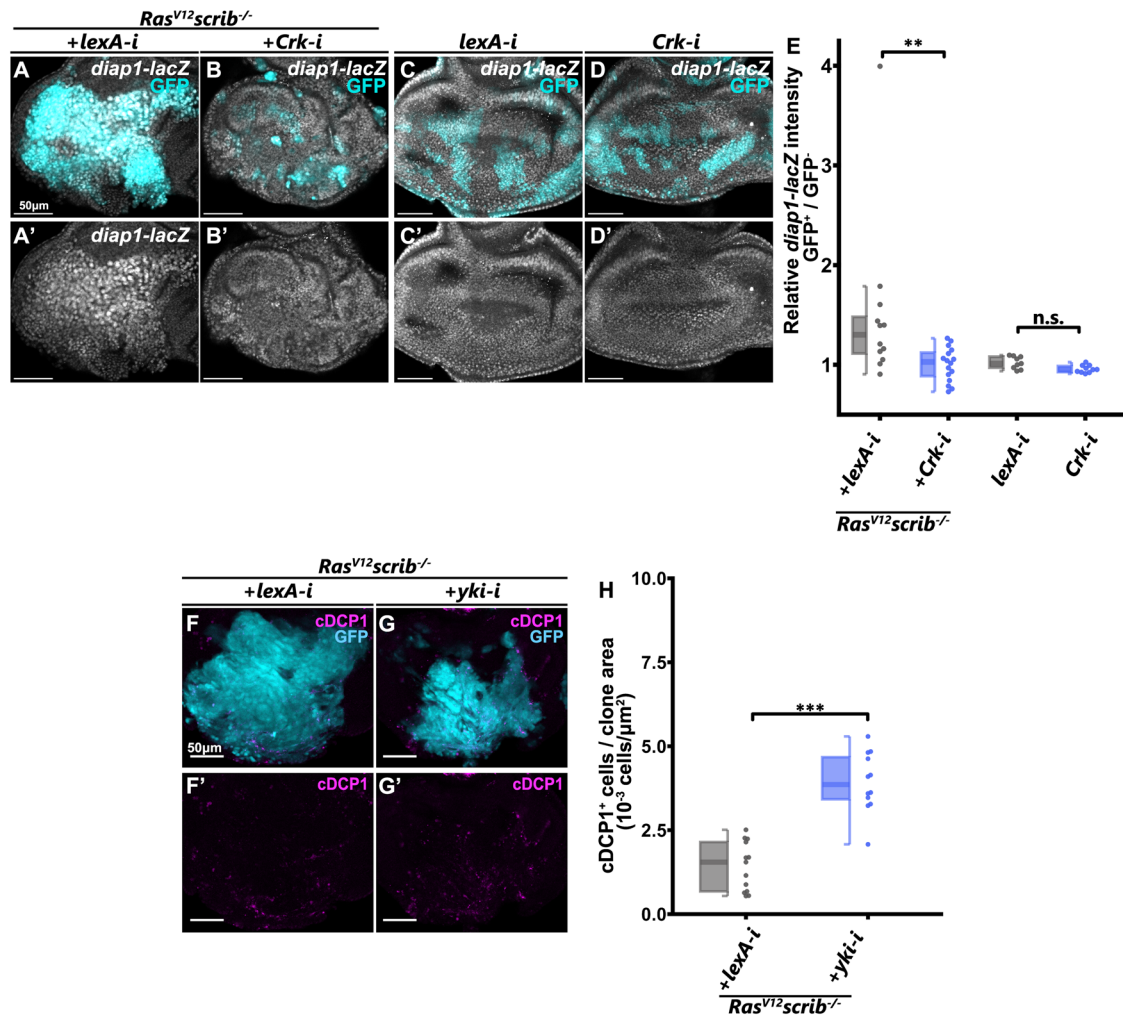


Fig. 3 | Loss of Crk suppresses Yki/YAP1 activity in *Ras^{V12}/scrib^{-/-}* tumors. A–D Eye disc bearing eyFLP-induced MARCM clones and *diap1-lacZ* heterozygosity of *Ras^{V12} + scrib^{-/-} + lexA-i* (A), *Ras^{V12} + scrib^{-/-} + Crk-i* (B), *lexA-i* (C), *Crk-i* (D) cells stained with anti-β-galactosidase. Scale bars, 50μm. E Box plot overlaid with dot plot represents the relative intensity of *diap1-lacZ* in clone for *Ras^{V12} + scrib^{-/-} + lexA-i* (n = 12), *Ras^{V12} + scrib^{-/-} + Crk-i* (n = 16), *lexA-i* (n = 9), *Crk-i* (n = 10) clones. Each plot corresponds to the raw data. Statistical significance is

shown as follows: **p < 0.01; n.s. (not significant) p > 0.05; Wilcoxon rank sum test. F, G Eye disc bearing eyFLP-induced MARCM clones of *Ras^{V12} + scrib^{-/-} + lexA-i* (F), *Ras^{V12} + scrib^{-/-} + yki-i* (G) cells stained with anti-cleaved Dcp-1. Scale bars, 50μm. H Box plot overlaid with dot plot represents the number of c-Dcp1 positive cells in clone for *Ras^{V12} + scrib^{-/-} + lexA-i* (n = 13), *Ras^{V12} + scrib^{-/-} + yki-i* (n = 12) clones. Each plot corresponds to the raw data. Statistical significance is shown as follows: ***p < 0.001; Wilcoxon rank sum test.

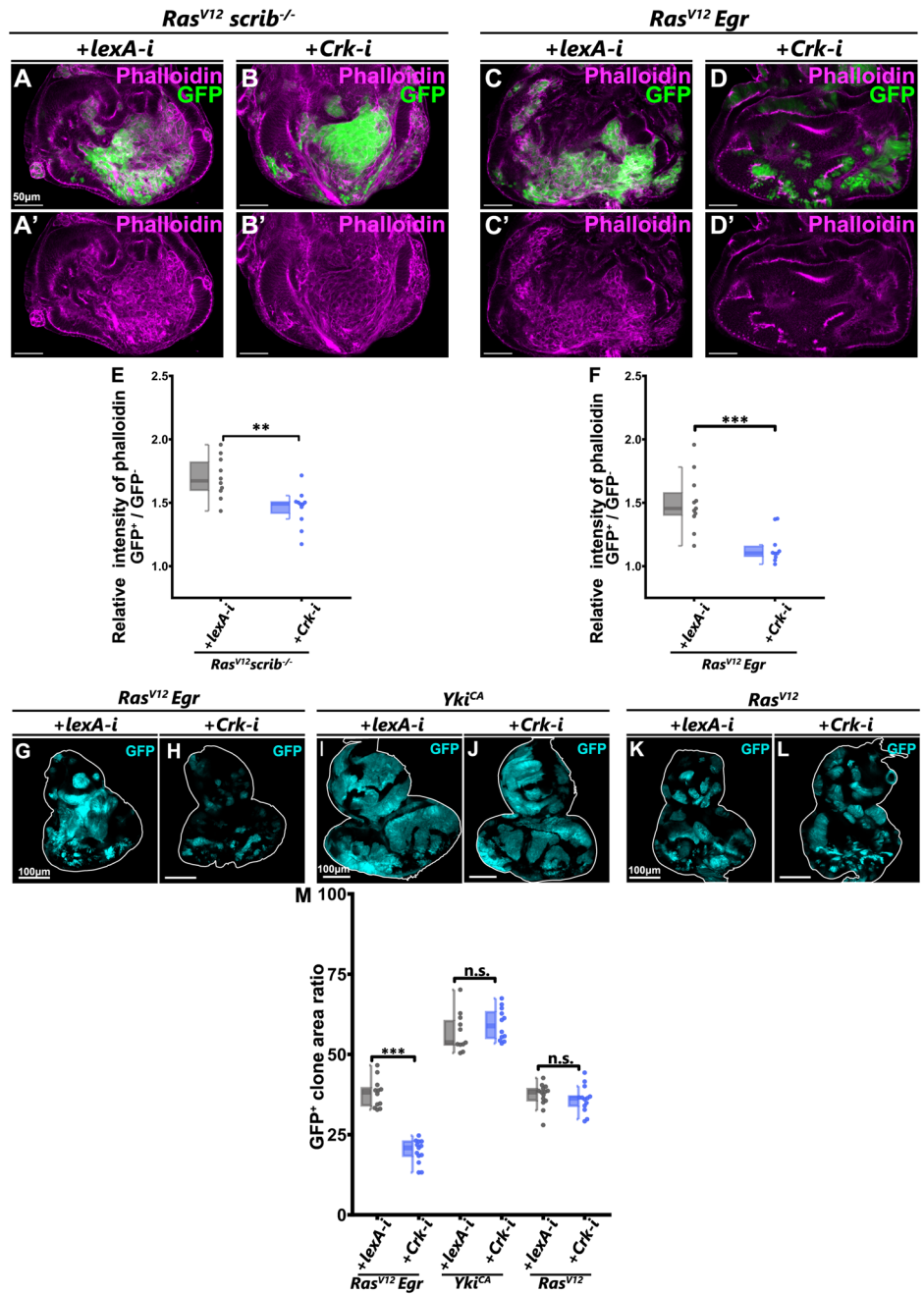
in *Ras^{V12}/scrib^{-/-}* malignant tumors downregulates Yki/YAP activity by impairing intracellular F-actin accumulation, which causes elevated JNK signaling to be used for JNK-dependent cell death induction (Fig. 6). Subsequent database analysis revealed that YAP-activated human cancers are sensitive to loss of CRK or CRKL. These data propose that CRK family proteins can be a rational therapeutic target for YAP-activated cancers.

Previous studies have shown the mechanisms of how CRK and CRKL contribute to carcinogenesis and how their inhibitions suppress cancers. For instance, CRK causes Src-dependent MAPK activation, which promotes synovial sarcoma proliferation³⁴. CRK promotes epithelial-mesenchymal transition (EMT) of colorectal cancer and metastasis of bladder cancer^{35,36}. However, the mechanisms by which CRK inhibition suppresses cancer development and progression have been elusive. By taking advantages of the *Drosophila* genetic techniques, we found that Crk inhibition blocks Yki/YAP activity, thereby causing JNK-dependent cell death in malignant tumors. While JNK signaling is known to promote tumorigenesis in many contexts, it has also been shown to suppress tumorigenesis in different contexts and JNK is expected to be a therapeutic target^{37,38}. For instance, JNK activation triggered by several compounds (e.g., Rhein, Propranolol, and Saikosaponin D) induces apoptosis in cancer cells in vitro^{39–41}. In addition,

hyper-activation of JNK signaling suppresses Ras-activated malignant tumors by inducing apoptosis in *Drosophila*⁴². Future studies should address whether the mechanism of JNK-mediated cell death induction by CRK inhibition is conserved in human cancers.

YAP is a promising target for cancer therapy and thus recent studies have focused on manipulating YAP activity by inhibiting the interaction between YAP and TEAD, a transcription factor that acts with YAP⁴³. However, YAP also interacts with several proteins other than TEAD^{8,44,45}, which include mutant p53 and β-catenin thereby promotes cancer cell proliferation and survival^{46,47}. Therefore, an alternative approach to effectively eliminate YAP-activated cancer is to block upstream or downstream molecules of YAP. Our study in *Drosophila* proposes that CRK family proteins are such target molecules. Although direct inhibitors of CRK family proteins have not been developed yet, several approaches targeting CRK family proteins or their downstream effectors are in trial. For instance, a synthetic peptide that inhibits the phosphorylation of CRK by ABL kinase, an upstream kinase of CRK in mammals, was designed based on the protein structure⁴⁸. In addition, an inhibitor of Ras-associated protein-1 (Rap1), a downstream effector of CRK, has been shown to suppress cell survival and proliferation of colon cancer cells in vitro³⁵. The SH2 and SH3 domains of

Fig. 4 | Loss of Crk suppresses malignant tumors by impairing F-actin accumulation. A, B Eye disc bearing eyFLP-induced MARCM clones of *Ras^{V12} + scrib^{-/-} + lexA-i* (A), *Ras^{V12} + scrib^{-/-} + Crk-i* (B) cells stained with Phalloidin. Dissections were performed at day 6 after egg laying. Scale bars, 100µm. C, D Eye disc bearing eyFLP-induced MARCM clones of *Ras^{V12} + Egr + lexA-i* (C), *Ras^{V12} + Egr + Crk-i* (D) cells stained with Phalloidin. Dissections were performed at day 6 after egg laying. Scale bars, 100µm. E Box plot overlaid with dot plot represents the relative intensity of Phalloidin in clone for *Ras^{V12} + scrib^{-/-} + lexA-i* (n = 10), *Ras^{V12} + scrib^{-/-} + Crk-i* (n = 11) Each plot corresponds to the raw data. Statistical significance is shown as follows: **p < 0.01; Wilcoxon rank sum test. F Box plot overlaid with dot plot represents the relative intensity of Phalloidin in clone for *Ras^{V12} + Egr + lexA-i* (n = 11), *Ras^{V12} + Egr + Crk-i* (n = 10). Each plot corresponds to the raw data. Statistical significance is shown as follows: ***p < 0.001; Wilcoxon rank sum test. G–L Eye disc bearing eyFLP-induced MARCM clones of *Ras^{V12} + Egr + lexA-i* (G), *Ras^{V12} + Egr + Crk-i* (H), *Yki^{CA} + lexA-i* (I), *Yki^{CA} + Crk-i* (J), *Ras^{V12} + lexA-i* (K), *Ras^{V12} + Crk-i* (L) cells. Scale bars, 100µm. M Box plot overlaid with dot plot represents the total GFP-positive clone area per total disc area (the proportion of total clone area/ disc area of the eye-antennal disc) for *Ras^{V12} + Egr + lexA-i* (n = 12), *Ras^{V12} + Egr + Crk-i* (n = 13), *Yki^{CA} + lexA-i* (n = 11), *Yki^{CA} + Crk-i* (n = 12), *Ras^{V12} + lexA-i* (n = 14), *Ras^{V12} + Crk-i* (n = 13) clones. Each plot corresponds to the raw data. Statistical significance is shown as follows: ***p < 0.001; n.s. (not significant) p > 0.05; Wilcoxon rank sum test.



CRK family proteins¹⁶ have been expected to be the potential targets of drug-mediated modulation to block downstream signal transduction^{17,49,50}.

Given that molecules and intracellular signaling pathways we identified in *Drosophila* are highly conserved and frequently activated in human cancers, future studies based on our findings may provide an ideal anticancer strategy for YAP-activated human cancers.

Methods

Fly strain and generation of clones

Drosophila melanogaster strains were raised in vials containing a standard cornmeal-yeast food maintained at 25 °C. For the generation of mitotic clones with gene mutations or transgenes, 20–30 virgin females of healthy tester strains were crossed to about 10 healthy males for mating, then transferred to new vials for subsequent egg-laying. Egg-laying was allowed for 8–12 h to uniform the developmental stage of the third instar larvae. Males and females at the wandering third instar larval stage were collected for each assay, except in analyses of flies that bore transgenes on the

X chromosome. No phenotypic differences were observed due to sex differences. For genetic screening and subsequent analysis, fluorescently-labeled mitotic clones were induced into larval eye-antenna imaginal discs using MARCM technique.

Mosaic clones were induced with strains as follows:

w; eyFLP, Act > y + >Gal4, UAS-GFP / CyO; FRT82B, tub-Gal80, / TM6B, Tb (82B MARCM tester)

w; eyFLP, Act > y + >Gal4, UAS-GFP / CyO; diap1-lacZ, FRT82B, tub-Gal80, / TM6B, Tb (diap1-lacZ 82B MARCM tester)

UAS-Bsk^{DN}, eyFLP, Act > y + >Gal4, UAS-GFP / CyO; diap1-lacZ, FRT82B, tub-Gal80, / TM6B, Tb (Bsk^{DN} 82B MARCM tester)

UAS-p35; eyFLP, Act > y + >Gal4, UAS-GFP / CyO; diap1-lacZ, FRT82B, tub-Gal80, / TM6B, Tb (p35 82B MARCM tester)

eyFLP, UAS-Dcr2; Act > y + >Gal4, UAS-mCherry; FRT82B, tub-Gal80 / T(2:3)SM5-TM6 (82B MARCM mCherry tester)

tub-Gal80, FRT19A; UAS-Ras^{V12}, UAS-Eiger; eyFLP, Act > y + >Gal4, UAS-GFP (Ras/Egr 19 A MARCM tester)

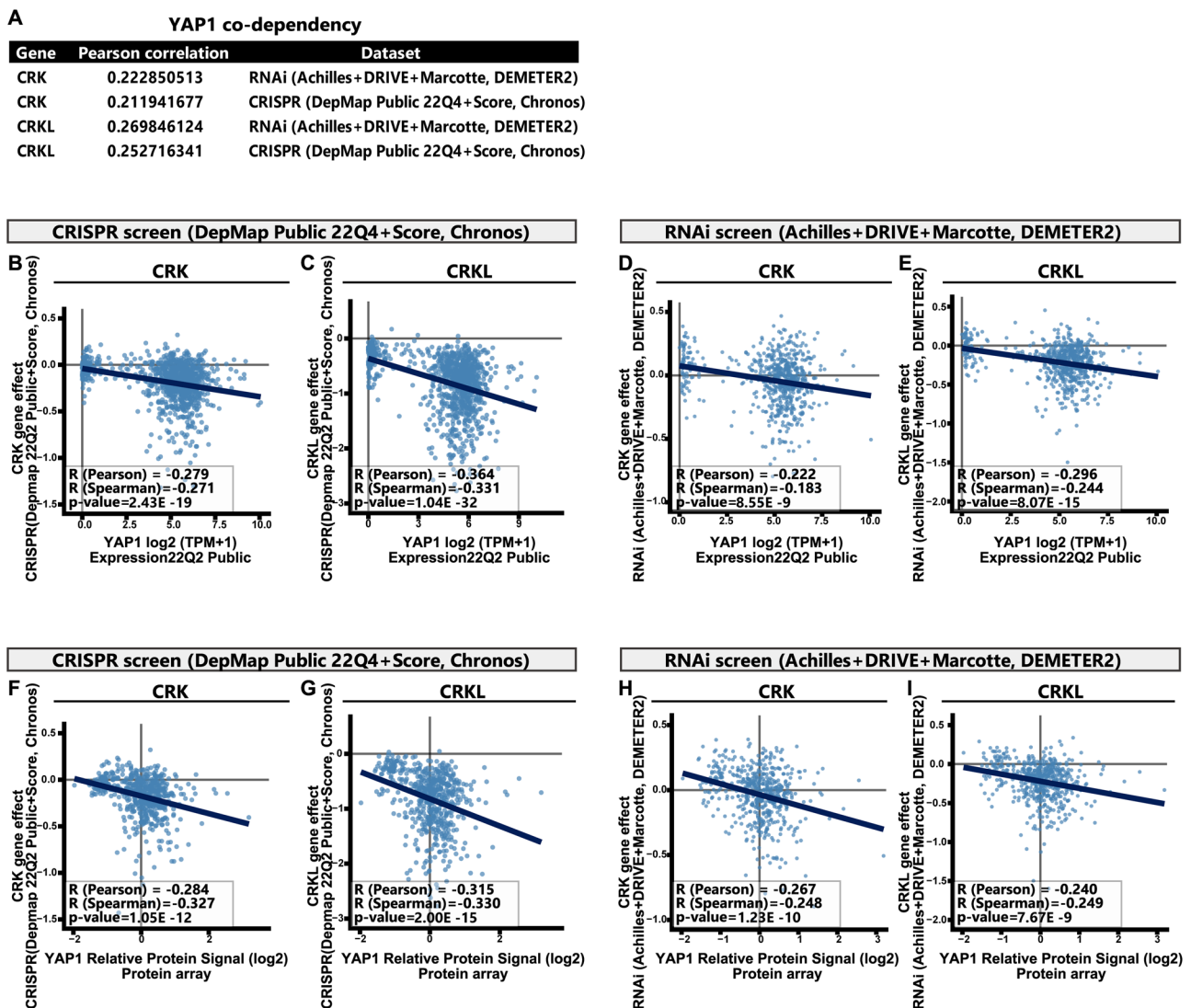


Fig. 5 | Data analysis of the human cancer cell lines. A Pearson correlation values for YAP1 and CRK or YAP1 and CRKL dependency scores. B–E Plot of the dependency score of CRK or CRKL (y-axis) against YAP1 transcript expression (x-axis). Plot of the dependency score of CRK (B), and CRKL (C) against YAP1 transcript expression in CRISPR screen. Plot of the dependency score of CRK (D), and CRKL (E) against YAP1 transcript expression in RNAi screen. F–I Plot of the dependency score of CRK or CRKL (y-axis) against YAP1 protein expression (x-axis). Plot of the dependency score of CRK (F), and CRKL (G) against YAP1 protein expression in CRISPR screen. Plot of the dependency score of CRK (H), and CRKL (I) against YAP1 protein expression in RNAi screen.

tub-Gal80, FRT19A; UAS-Yki^{CA}; eyFLP, Act > y + >Gal4, UAS-GFP (Yki^{CA} 19A MARCM tester)

tub-Gal80, FRT19A; UAS-lexA-RNAi; eyFLP, Act > y + >Gal4, UAS-GFP (lexA-RNAi 19A MARCM tester) tub-Gal80, FRT19A; UAS-Crk-RNAi; eyFLP, Act > y + >Gal4, UAS-GFP (Crk-RNAi 19A MARCM tester)

Other strains used for analyses are as follows: *UAS-Ras^{V12}6, scrib¹* (a gift from David Bilder), *dlg^{ms2}* (a gift from Scott Goode⁵²), *UAS-Bsk^{DNS1}*, *UAS-Yki^{CA}* (BDSC #28836), *UAS-Yki^{CA}* (BDSC #28818), *UAS-p35* (a gift from Marcos González-Gaitán), *UAS-Eiger²⁹*, *UAS-Crk-RNAi* (BDSC #55277), *UAS-lexA-RNAi* (BDSC #67947), *UAS-yki-RNAi* (NIG #4005R-2), *mNG::3XFLAG::Crk* (BDSC #83700), *diap1-lacZ/ Diap1^{J5C8}* (BDSC #12093), *eyFLP, UAS-Dcr2* (BDSC #58757), *ex697 (ex-lacZ)* (BDSC # 44248), *UAS-lacZ* (BDSC #8529), *UAS-Crk* (BDSC # 83704). Detailed genotypes used in this study are provided in Supplementary Table 2.

Genetic screening

For RNAi screen, RNAi strains for genes located on the *Drosophila* 4th chromosome were chosen. The list of strains are provided in Supplementary Table 1. More than 10 virgin healthy strains were crossed to about 5–10

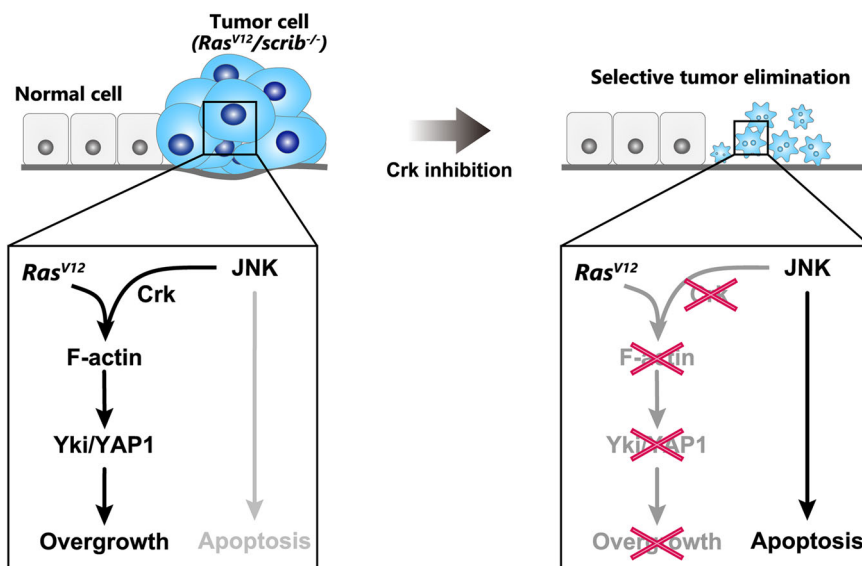
healthy males and grown at 25 °C. 7 days after egg-laying, observation was conducted. Tumor-suppressor strains were isolated by observing GFP-labeled tumor clone size induced in larval imaginal discs with M80 stereo microscope (Leica microsystems).

Immunohistochemistry

Wandering third instar larvae were dissected and fixed with 4% paraformaldehyde for 20 min at room temperature and washed with PBT (PBS containing 0.1% Triton X-100 solution) three times. Dissection of tumor-bearing larvae was performed 7 days after egg laying to assess tumor size. For immunostaining, dissection was performed 6 days after egg laying. For immunostaining, samples were incubated at 4 °C overnight with primary antibodies and then incubated with secondary antibody 2 h at RT.

Primary antibodies used are as follows: chicken anti-β-galactosidase (Abcam, # ab9361, 1:1000), rabbit anti-cleaved *Drosophila* Dcp1 (Asp216) (Cell Signaling Technology, # 9578, 1:100), mouse anti-Mmp1 (Developmental Studies Hybridoma Bank, # 3B8, # 3A6 and # 5H7 (mixture 1:1:1), 1:100), rabbit Phospho-SAPK/JNK (Thr183/Tyr185) (Cell Signaling

Fig. 6 | A model for tumor suppression caused by targeting Crk family proteins. *Drosophila* Crk, the ortholog of Human CRK and CRKL, is expressed in Ras-activated polarity-deficient tumors (*Ras^{V12}+scrib^{-/-}*). Crk in *Ras^{V12}+scrib^{-/-}* tumors contributes to the F-actin accumulation, resulting in Yki/YAP1 activation. Inhibition of Crk in tumors increases apoptosis in a JNK signaling-dependent manner, while it doesn't affect wild-type cells.



Technology, #9255, 1:200), mouse anti-GFP (MEDICAL & BIOLOGICAL LABORATORIES, # D153-A48, 1:200), Alexa Fluor™ 546 Phalloidin (Invitrogen, # A22283, 1:200).

Secondary antibodies used are as follows: Goat anti-Chicken IgY (H + L) Secondary Antibody, Alexa Fluor 555 (Thermo Fisher Scientific, # A-21437, 1:250), Goat anti-Rabbit IgG (H + L) Highly Cross-Adsorbed Secondary Antibody, Alexa Fluor 546 (Thermo Fisher Scientific, # A-11035, 1:250), Goat anti-Mouse IgG (H + L) Highly Cross-Adsorbed Secondary Antibody, Alexa Fluor 546 (Thermo Fisher Scientific, # A-11030, 1:250).

EdU staining

Detection of 5-ethynyl-2-deoxyuridine (EdU) was performed with Click-iT Plus EdU Alexa Fluor 647 Imaging Kit (Thermo Fisher Scientific, #C10640). Five to seven wandering third instar larvae were dissected in Schneider's *Drosophila* medium (Thermo Fisher Scientific) with 5% FBS, and incubated in 100 μ M EdU for 120 min. After EdU incorporation, larvae were fixed in 4% paraformaldehyde for 20 min at room temperature and EdU was detected by following manufacturer's manual.

Image acquisition

Confocal images were taken with a confocal microscope ZEISS LSM 880 (Carl Zeiss) under the control of ZEN Blue (Carl Zeiss). For the subsequent captured image processing, ZEN 3.6 blue edition (Carl Zeiss) was used. Confocal images of Supplementary Fig. 1–8 were taken with Laser Scanning Confocal Microscope TCS SP8 on DMi8 inverted microscope (Leica Microsystems) controlled with Leica Application Suite X version 3.5.5.19976 (Leica Microsystems).

Quantification

X.Y. confocal images of the imaginal discs stained with corresponding antibodies and DAPI were acquired and processed using FIJI ImageJ-win64 (ver. 1.54 f). The subsequent analysis was differentiated depending on the antibodies used for staining.

For measurement of cDCP1 positive cells inside GFP positive cells:

The number of cDCP1-positive cells inside the GFP positive cells is quantified. Then, area of GFP positive clone was quantified as “total GFP⁺ clone area.” The ratio cDCP1⁺ cells / GFP⁺ clone area was calculated and defined as “cDCP1⁺ cells/ clone area”.

For measurement of cDCP1 positive cells in GFP negative cells of the tissue:

The number of cDCP1-positive cells in the GFP negative cells of the tissue is quantified. Then, area of GFP negative are was quantified as “total

GFP⁻ area.” The ratio cDCP1⁺ cells / GFP⁻ clone area was calculated and defined as “cDCP1⁺ cells/ GFP⁻ area”.

For measurement of Phalloidin, pJNK, *ex-lacZ*, *diap1-lacZ*, EdU, and Mmp1 staining intensity:

The mean gray value of GFP-labeled tumors were quantified as “Signal intensity (GFP⁺)”. Then mean gray value of the outside of GFP positive area within the tissue (Eye-disc region) was quantified as “Signal intensity (GFP⁻)”. The ratio “Signal intensity (GFP⁺)” / “Signal intensity (GFP⁻)” was calculated and defined as “Relative intensity of Signal (GFP⁺/GFP⁻)”.

Depmap database analysis

For analyzing the correlation between YAP expression (*YAP* transcript or YAP protein level) and CRK or CRKL gene effect, the original data were downloaded from the database of the Cancer Dependency Map project (DepMap portal: <https://depmap.org/portal>). Linear regression analysis was performed on DepMap Data Explorer (<https://depmap.org/portal/interactive/>). Top 100 co-dependent genes with YAP were downloaded from YAP overview page (<https://depmap.org/portal/gene/YAP1?tab=overview>). Pearson correlation score is described as co-dependency score. Original data are provided in Supplementary Data.

Statistics and reproducibility

Wilcoxon rank sum test for single comparisons was adopted appropriately and performed. Details of statistical evaluations and the numbers of samples were written in the each figure legend. Sample size adjustment was not performed by predetermining test. Each plot represents biological replicates and each experiment was independently performed at least three times. All analyses and data visualization were performed using R (ver. 3.4.1) on RStudio (Ver. 1.0.153). Significances are shown as follows. *: $p < 0.05$, **: $p < 0.01$ ***, $p < 0.001$, n.s. (not significant): $p > 0.05$.

Reporting summary

Further information on research design is available in the Nature Portfolio Reporting Summary linked to this article.

Data availability

All data reported in this paper will be shared by the lead contact upon request. Data behind the graph are provided in Supplementary Data. Any additional information required to reanalyze the data reported in this paper is available from the lead contact upon request.

Code availability

This paper does not include original code.

Received: 7 January 2024; Accepted: 13 September 2024;
Published online: 28 September 2024

References

- Jiang, H., Kimura, T., Hai, H., Yamamura, R. & Sonoshita, M. Drosophila as a toolkit to tackle cancer and its metabolism. *Front. Oncol.* **12**, 982751 (2022).
- La Marca, J. E. et al. A Drosophila chemical screen reveals targeting MEK and DGKα mitigates Ras-driven polarity-impaired tumour growth. *Dis. Model. Mech.* <https://doi.org/10.1242/dmm.049769> (2023).
- Bangi, E., Murgia, C., Teague, A. G. S., Sansom, O. J. & Cagan, R. L. Functional exploration of colorectal cancer genomes using Drosophila. *Nat. Commun.* **7**, 1–16 (2016).
- Lee, T. & Luo, L. Mosaic analysis with a repressible cell marker for studies of gene function in neuronal morphogenesis. *Neuron* **22**, 451–461 (1999).
- Pagliarini, R. A. & Xu, T. A genetic screen in drosophila for metastatic behavior. *Science* **302**, 1227–1231 (2003).
- Igaki, T., Pagliarini, R. A. & Xu, T. Loss of cell polarity drives tumor growth and invasion through JNK activation in drosophila. *Curr. Biol.* **16**, 1139–1146 (2006).
- Mirzoyan, Z. et al. Drosophila melanogaster: a model organism to study cancer. *Front. Genet.* **10**, 51 (2019).
- Szulzewsky, F., Holland, E. C. & Vasioukhin, V. YAP1 and its fusion proteins in cancer initiation, progression and therapeutic resistance. *Dev. Biol.* **475**, 205–221 (2021).
- Zanconato, F., Cordenonsi, M. & Piccolo, S. YAP/TAZ at the roots of cancer. *Cancer Cell* **29**, 783–803 (2016).
- Cunningham, R. & Hansen, C. G. The Hippo pathway in cancer: YAP/TAZ and TEAD as therapeutic targets in cancer. *Clin. Sci* **136**, 197–222 (2022).
- Zhang, Y., Wang, X. & Zhou, X. Functions of Yes-association protein (YAP) in cancer progression and anticancer therapy resistance. *Brain Sci. Adv.* **8**, 1–18 (2022).
- Luo, J. et al. The oncogenic roles and clinical implications of YAP/TAZ in breast cancer. *Br. J. Cancer.* <https://doi.org/10.1038/s41416-023-02182-5> (2023).
- Huang, J., Wu, S., Barrera, J., Matthews, K. & Pan, D. The Hippo signaling pathway coordinately regulates cell proliferation and apoptosis by inactivating Yorkie, the Drosophila homolog of YAP. *Cell* **122**, 421–434 (2005).
- Snigdha, K., Gangwani, K. S., Lalalikar, G. V., Singh, A. & Kango-Singh, M. Hippo signaling in cancer: Lessons from Drosophila models. *Fron. Cell Dev. Biol.* <https://doi.org/10.3389/fcell.2019.00085> (2019).
- Feller, S. M. Crk family adaptors—signalling complex formation and biological roles. *Oncogene* **20**, 6348–6371 (2001).
- Birge, R. B., Kalodimos, C., Inagaki, F. & Tanaka, S. Crk and CrkL adaptor proteins: networks for physiological and pathological signaling. *Cell Communication and Signaling* **7**, 1–23 (2009). 2009 7:1.
- Park, T. Crk and CrkL as therapeutic targets for cancer treatment. *Cells* **10**, 739 (2021).
- Tsuda, M. & Tanaka, S. Roles for crk in cancer metastasis and invasion. *Genes Cancer* **3**, 334–340 (2012).
- Spracklen, A. J. et al. The Crk adapter protein is essential for Drosophila embryogenesis, where it regulates multiple actin-dependent morphogenic events. *Mol. Biol. Cell* **30**, 2399–2421 (2019).
- Xu, T. & Rubin, G. M. Analysis of genetic mosaics in developing and adult Drosophila tissues. *Development* **117**, 1223–1237 (1993).
- Cong, B. et al. JNK and Yorkie drive tumor malignancy by inducing L-amino acid transporter 1 in Drosophila. *PLoS Genet.* **17**, e1009893 (2021).
- Uhlirva, M. & Bohmann, D. JNK- and Fos-regulated Mmp1 expression cooperates with Ras to induce invasive tumors in Drosophila. *EMBO J.* **25**, 5294–5304 (2006).
- Igaki, T. et al. Eiger, a TNF superfamily ligand that triggers the Drosophila JNK pathway. *EMBO J.* **21**, 3009–3018 (2002).
- Moreno, E., Yan, M. & Basler, K. Evolution of TNF signaling mechanisms: JNK-dependent apoptosis triggered by Eiger, the Drosophila homolog of the TNF superfamily. *Curr. Biol.* **12**, 1263–1268 (2002).
- Igaki, T., Pastor-Pareja, J. C., Aonuma, H., Miura, M. & Xu, T. Intrinsic tumor suppression and epithelial maintenance by endocytic activation of eiger/TNF signaling in drosophila. *Dev. Cell* **16**, 458–465 (2009).
- Atkins, M. et al. An ectopic network of transcription factors regulated by hippo signaling drives growth and invasion of a malignant tumor model. *Curr. Biol.* **26**, 2101–2113 (2016).
- Doggett, K., Grusche, F. A., Richardson, H. E. & Brumby, A. M. Loss of the Drosophila cell polarity regulator Scribbled promotes epithelial tissue overgrowth and cooperation with oncogenic Ras-Raf through impaired Hippo pathway signaling. *BMC Dev. Biol.* **11**, 57 (2011).
- Hamaratoglu, F. et al. The tumour-suppressor genes NF2/Merlin and Expanded act through Hippo signalling to regulate cell proliferation and apoptosis. *Nat. Cell Biol.* **8**, 27–36 (2006).
- Enomoto, M., Kizawa, D., Ohsawa, S. & Igaki, T. JNK signaling is converted from anti- to pro-tumor pathway by Ras-mediated switch of Warts activity. *Dev. Biol.* **403**, 162–171 (2015).
- Dong, J. et al. Elucidation of a universal size-control mechanism in Drosophila and mammals. *Cell* **130**, 1120–1133 (2007).
- Oh, H. & Irvine, K. D. In vivo regulation of Yorkie phosphorylation and localization. *Development* **135**, 1081–1088 (2008).
- Meyers, R. M. et al. Computational correction of copy number effect improves specificity of CRISPR-Cas9 essentiality screens in cancer cells. *Nat. Genet.* **49**, 1779–1784 (2017).
- McFarland, J. M. et al. Improved estimation of cancer dependencies from large-scale RNAi screens using model-based normalization and data integration. *Nat. Commun.* **9**, 4610 (2018).
- Watanabe, T. et al. Adaptor protein Crk induces Src-dependent activation of p38 MAPK in regulation of synovial sarcoma cell proliferation. *Mol. Cancer Res.* **7**, 1582–1592 (2009).
- Franke, F. C. et al. Novel role for CRK adaptor proteins as essential components of SRC/FAK signaling for epithelial–mesenchymal transition and colorectal cancer aggressiveness. *International Journal of Cancer* **147**, 1715–1731 (2020).
- Yoshida, K. et al. Exosomes containing ErbB2/CRK induce vascular growth in premetastatic niches and promote metastasis of bladder cancer. *Cancer Sci* **110**, 2119–2132 (2019).
- Wu, Q. et al. JNK signaling in cancer cell survival. *Med. Res. Rev.* **39**, 2082–2104 (2019).
- Tournier, C. The 2 Faces of JNK Signaling in Cancer. *Genes Cancer* **4**, 397–400 (2013).
- Wang, A. et al. Rhein induces liver cancer cells apoptosis via activating ROS-dependent JNK/Jun/caspase-3 signaling pathway. *J. Cancer* **11**, 500 (2020).
- Lai, M. et al. Saikosaponin D Inhibits Proliferation and Promotes Apoptosis Through Activation of MKK4-JNK Signaling Pathway in Pancreatic Cancer Cells. *Onco. Targets. Ther.* **13**, 9465–9479 (2020).
- Zhao, S. et al. Propranolol induced apoptosis and autophagy via the ROS/JNK signaling pathway in Human Ovarian Cancer. *J. Cancer* **11**, 5900–5910 (2020).
- Wang, Z., Xia, X., Li, J. & Igaki, T. Tumor elimination by clustered microRNAs miR-306 and miR-79 via noncanonical activation of JNK signaling. *Elife* **11**, e77340 (2022).
- Calses, P. C., Crawford, J. J., Lill, J. R. & Dey, A. Hippo pathway in cancer: aberrant regulation and therapeutic opportunities. *Trends Cancer Res.* **5**, 297–307 (2019).
- Pan, D. The hippo signaling pathway in development and cancer. *Dev. Cell* **19**, 491–505 (2010).
- Totaro, A., Panciera, T. & Piccolo, S. YAP/TAZ upstream signals and downstream responses. *Nat. Cell Biol.* **20**, 888–899 (2018).

46. Di Agostino, S. et al. YAP enhances the pro-proliferative transcriptional activity of mutant p53 proteins. *EMBO Rep.* **17**, 188–201 (2016).
47. Rosenbluh, J. et al. β -Catenin-driven cancers require a YAP1 transcriptional complex for survival and tumorigenesis. *Cell* **151**, 1457–1473 (2012).
48. Shen, Q., Bhatt, V. S., Krieger, I., Sacchettini, J. C. & Cho, J.-H. Structure-guided design of a potent peptide inhibitor targeting the interaction between CRK and ABL kinase. *Medchemcomm* **9**, 519–524 (2018).
49. Diop, A. et al. SH2 domains: Folding, binding and therapeutical approaches. *Int. J. Mol. Sci.* **23**, 15944 (2022).
50. Nardella, C. et al. Folding and binding mechanisms of the SH2 domain from Crkl. *Biomolecules* **12**, 1014 (2022).
51. Adachi-Yamada, T., Fujimura-Kamada, K., Nishida, Y. & Matsumoto, K. Distortion of proximodistal information causes JNK-dependent apoptosis in Drosophila wing. *Nature* **400**, 166–169 (1999).
52. Goode, S. & Perrimon, N. Inhibition of patterned cell shape change and cell invasion by Discs large during Drosophila oogenesis. *Genes Dev* **11**, 2532–2544 (1997).

Acknowledgements

The authors thank K. Taniguchi and M. Enomoto for discussions; M. Nishiyama for providing EdU assay protocol; M. Nakamura, Y. Sando, K. Gomi, M. Matsuoka, M. Sada and M. Kojima for technical support; the Bloomington Drosophila Stock Center (BDSC, Indiana, USA), the Vienna Drosophila Resource Center (VDRC, Vienna, Austria), the Drosophila Genomics and Genetic Resources (DGGR, Kyoto, Japan), and National Institute of Genetics (NIG, Shizuoka, Japan) for providing fly stocks. This work was supported in part by grants from the MEXT/JSPS KAKENHI (21H05284 and 21H05039) to T.I., AMED-CREST, Japan Agency for Medical Research and Development (22gm1710002h0001) to T.I., the Takeda Science Foundation to T.I., and the Naito Foundation to T.I. B.K. was supported by JSPS Research Fellowship for Young Scientists.

Author contributions

B.K. and T.I. designed screens, B.K. conducted screens, B.K. designed and conducted subsequent experiments with input from T.I., B.K. and T.I. analyzed the data, and B.K. and T.I. wrote the manuscript.

Competing interests

The authors declare no competing interests.

Additional information

Supplementary information The online version contains supplementary material available at <https://doi.org/10.1038/s42003-024-06897-w>.

Correspondence and requests for materials should be addressed to Tatsushi Igaki.

Peer review information *Communications Biology* thanks Xianfeng Wang, Xianjue Ma and the other, anonymous, reviewer(s) for their contribution to the peer review of this work. Primary Handling Editors: Jun Wei Pek and Manuel Breuer.

Reprints and permissions information is available at <http://www.nature.com/reprints>

Publisher's note Springer Nature remains neutral with regard to jurisdictional claims in published maps and institutional affiliations.

Open Access This article is licensed under a Creative Commons Attribution-NonCommercial-NoDerivatives 4.0 International License, which permits any non-commercial use, sharing, distribution and reproduction in any medium or format, as long as you give appropriate credit to the original author(s) and the source, provide a link to the Creative Commons licence, and indicate if you modified the licensed material. You do not have permission under this licence to share adapted material derived from this article or parts of it. The images or other third party material in this article are included in the article's Creative Commons licence, unless indicated otherwise in a credit line to the material. If material is not included in the article's Creative Commons licence and your intended use is not permitted by statutory regulation or exceeds the permitted use, you will need to obtain permission directly from the copyright holder. To view a copy of this licence, visit <http://creativecommons.org/licenses/by-nc-nd/4.0/>.

© The Author(s) 2024